Data Paper

Laboratory Experiments of Vertical Cylinders Representative of Aboveground Storage Tanks Subjected to Waves

Carl Bernier, S.M.ASCE[1]; Jamie E. Padgett, A.M.ASCE[2]; Yuxiang Lin[3]; Clint N. Dawson[4]; Pedro Lomonaco[5]; and Daniel T. Cox, M.ASCE[6]

Abstract: This paper presents an overview of laboratory experiments of vertical cylinders representative of aboveground storage tanks (ASTs) subjected to waves. The main objective is to provide an experimental dataset for the validation of finite element models of cylindrical structures subjected to wave loads during storm surge events. Four types of waves were considered in the experiments: regular waves, random waves, solitary waves, and double solitary waves. To investigate the interference created by an adjacent cylinder, three different configurations of the experiment were considered: a single test cylinder, a dummy cylinder located in front of the test cylinder, and no cylinders. The experimental data consist of pressures and wave runups recorded on the test cylinder and water surface elevations and water velocities recorded around the cylinders. This paper describes the experimental setup, experimental wave conditions, instrumentation, experimental plan, and curation process for open access of the experimental dataset. Samples and preliminary analyses of the experimental data are also presented to demonstrate the quality and relevance of the measurements for numerical benchmarking. **DOI: 10.1061/(ASCE)ST.1943-541X.0002611.**

Author keywords: Large cylinders; Storm surge; Wave loads; Hydraulic experiments; Wave basin.

Introduction and Background

Aboveground storage tanks (ASTs) are critical components of oil refineries, ports, terminals, and petrochemical facilities that allow the storage of large quantities of raw and refined liquids. However, their vulnerability was highlighted during recent hurricane and storm events in the United States. During Hurricanes Katrina and Rita in 2005, more than 26 million liters of oil were spilled into the environment due to AST failures (Godoy 2007). More recently during Hurricane Harvey in 2017, two ASTs released one million liters of gasoline in the Houston area (Eaton and Blum 2017). Post-hurricane reconnaissance reports usually identify three failure mechanisms for ASTs: (1) buckling of the tank shell due to wind load; (2) dislocation from the ground (flotation, overturning, or sliding) due to storm surge and wave effects; and (3) buckling of the tank shell due to storm surge and wave effects (Godoy 2007; Cozzani et al. 2010). To date, most of the existing literature has focused primarily on the structural safety of ASTs under hurricane winds rather than the failure modes related to storm surge (Kameshwar and Padgett 2018). However, given the significant consequences of AST failures, it is crucial to also assess the structural safety of ASTs under storm surge and associated waves.

The safety assessment of ASTs under storm surge first requires an adequate estimation of the loads acting on ASTs. Wave forces are needed to assess stability against dislocation, while dynamic pressure distributions are required to determine the buckling strength. In past decades, numerous efforts were made to evaluate wave forces and pressures on vertical cylindrical structures. Morison et al. (1950) presented a semi-empirical model to estimate the horizontal wave force on small-scale vertical cylinders, where the relative length [or cylinder diameter (D) to wavelength (L) ratio (i.e., D/L)] is smaller than 0.15. For larger-scale cylinders, such as ASTs for which the D/L ratio can vary between 0.2 and 2.0, wave diffraction effects can become significant and should be considered. The first diffraction model was presented by MacCamy and Fuchs (1954) and include only linear diffraction effects. To consider nonlinear diffraction effects, second-order diffraction theories (e.g., Akyildiz 1999; Kriebel 1990; Rahman and Heaps 1983) have been proposed. These theories provide better agreement with experimental results than linear diffraction theory and are generally valid for wave conditions similar to second-order Stokes waves (Kriebel 1992; Kriebel 1998). However, as detailed in this work, ASTs can be exposed to more nonlinear waves during storms. In this case, higher-order solutions are required, but deriving such solutions can be quite challenging and difficult. Instead, numerical methods, such as the finite volume method (FVM) or the finite element method (FEM), are usually employed to derive wave forces and pressure distributions around large-scale cylinders subjected to highly nonlinear waves (Chen et al. 2014; Hu et al. 2016).

[1]Graduate Research Assistant, Dept. of Civil and Environmental Engineering, Rice Univ., 6100 Main St., MS-318, Houston, TX 77005. ORCID: https://orcid.org/0000-0002-5207-1973

[2]Associate Professor, Dept. of Civil and Environmental Engineering, Rice Univ., 6100 Main St., MS-318, Houston, TX 77005 (corresponding author). Email: jamie.padgett@rice.edu

[3]Graduate Research Assistant, Dept. of Aerospace Engineering and Engineering Mechanics, Univ. of Texas at Austin, 2617 Wichita St., Austin, TX 78712.

[4]Professor, Dept. of Aerospace Engineering and Engineering Mechanics, Univ. of Texas at Austin, 2617 Wichita St., Austin, TX 78712. ORCID: https://orcid.org/0000-0001-7273-0684

[5]Director, O.H. Hinsdale Wave Research Laboratory, Oregon State Univ., 101 Kearney Hall, Corvallis, OR 97331. ORCID: https://orcid.org/0000-0001-6721-5688

[6]Professor, School of Civil and Construction Engineering, Oregon State Univ., 101 Kearney Hall, Corvallis, OR 97331.

Note. This manuscript was submitted on January 15, 2019; approved on October 15, 2019; published online on February 26, 2020. Discussion period open until July 26, 2020; separate discussions must be submitted for individual papers. This paper is part of the ***Journal of Structural Engineering***, © ASCE, ISSN 0733-9445.

Further, the load models discussed only consider an isolated cylinder, whereas multiple ASTs are expected within a refinery or oil terminal. Depending on the configuration, the effects of adjacent cylinders can reduce or amplify the wave loads acting on a given cylinder (Cong et al. 2015). Some analytical solutions (e.g., Linton and Evans 1990; McIver and Evans 1984) are available for arrays of cylinders, but these solutions are often limited to linear or low-order waves. Again, numerical methods are commonly employed to study wave loads on arrays of cylinders (Kamath et al. 2015; Wang and Wu 2010).

The use of numerical models to estimate wave loads requires validation against experimental results to ensure the adequacy of the modeling assumptions (i.e., meshing, boundary conditions, and turbulence model) and the accuracy of the solution. The first experiment to validate linear diffraction theory was performed by Laird (1955), followed by a series of additional experiments in subsequent years (Chakrabarti and Tam 1975; Chakrabarti et al. 1986; Hogben and Standing 1975; Johnson 1972; Mogridge and Jamieson 1976; Nagai 1973; Neelamani et al. 1989; Niedzwecki and Duggal 1992). Kriebel (1987) and Akyildiz (2002) then performed experiments to test nonlinear diffraction theories; their experiments covered a broader range of wave parameters than the previous ones. More recently, experiments on focused waves (Li et al. 2014), multidirectional irregular waves (Ji et al. 2015), and arrays of cylinders have also been performed (Ohl et al. 2001a, b; Cong et al. 2015; Contento et al. 2005).

However, the experiments in the literature were generally designed for offshore structures and wave conditions and are not representative of the wave conditions that could be encountered by onshore structures such as ASTs during storm surge events. This is particularly true for experiments on arrays of cylinders that mainly focus on deep water conditions and on smaller-scale cylinders than ASTs. Further, many of these experiments were not designed to validate finite element models, and important data required for adequate benchmarking were not measured or provided. For instance, while most of these experiments provide total wave forces, many do not provide or provide limited data about pressure distribution and wave runup; buckling analyses can be highly sensitive to the spatial variation of these two measurements. Finally, most of these experiments focus on regular waves, which are less representative of the waves observed during a storm. As a result of these factors, comprehensive experimental datasets for large-scale vertical cylinders, such as ASTs, during storm surge events are currently lacking.

To address this gap, experiments were performed at the O.H. Hinsdale Wave Research Laboratory as a collaboration between researchers from Rice University, The University of Texas at Austin, and Oregon State University. The main objectives of the experiments were to (1) collect a comprehensive benchmarking dataset of wave heights, pressures, runups, and water velocities for scaled cylinders subjected to regular, random, and solitary waves representative of the ones that could be observed at AST locations during storm surge events; and (2) investigate the interference created by a second scaled cylinder for additional numerical benchmarking and to guide future numerical and experimental efforts. The experiments were specifically designed to measure hydrodynamic loads on vertical cylinders representative of ASTs, and no attempts were made to capture the structural behavior (i.e., buckling or dislocation) of such cylinders. A secondary objective of the experiments was also to provide a test case for data curation in DesignSafe.CI, the web-based research platform of the Natural Hazards Engineering Research Infrastructure (NHERI) Network (Rathje et al. 2017). This paper presents the experimental methodology and a preliminary analysis of the experimental results. The first five sections detail the experimental setup, wave conditions, instrumentation, experimental plan, and data processing and curation in DesignSafe.CI that allow other researchers to easily access and reuse this dataset. Then, samples of experimental data and preliminary analyses regarding the interference effects of the second cylinder are presented to highlight the quality and relevance of the data. Finally, the conclusion discusses potential future numerical and experimental work using the experimental dataset.

Physical Model Setup and Wave Basin Bathymetry

The experiments summarized in this paper were conducted using the directional wave basin (DWB) at the O.H. Hinsdale Wave Research Laboratory (HRWL), Oregon State University via the National Science Foundation NHERI Network. The experimental setup is schematized in Fig. 1 and shown in Fig. 2(a). The DWB is 48.8 m long, 26.5 m wide, has a wall height of 2.1 m, and is constructed of smooth concrete. The DWB is equipped with a snake-type wavemaker composed of 30 actuators and 29 paddles connected by vertical hinges and is capable of reproducing regular, irregular, solitary, multidirectional, and user-defined waves. The wavemaker maximum stroke and velocity are 2.1 m and 2.0 m/s, respectively. The origin of the DWB coordinate system was fixed such that $x = 0$ corresponds to the wavemaker neutral position, $y = 0$ corresponds to the basin centerline, and $z = 0$ corresponds to the average floor elevation. The x-axis was positive onshore (i.e., away from the wavemaker), the y-axis positive was to the left when facing onshore, and the z-axis was positive upward. The bathymetry comprised a flat section of 22.06 m, followed by a 1:10 sloped beach to dissipate wave energy. For all experiments, the water level was fixed at 0.5 m.

The test specimen was an aluminum vertical cylinder with a diameter of 1.22 m, height of 1.82 m, and thickness of 4 mm. As detailed in the next section, the test specimen was a scaled model of ASTs with geometric scales varying between 1:4 and 1:14. Since the experiments focused on capturing hydrodynamic loads, only the diameter of the test specimen was to scale. Thus, the test specimen was representative of prototype ASTs with diameter between 4.9 and 17 m. All other properties of the test specimen, such as the thickness, were selected such that the cylinder behave rigidly. As shown in Fig. 1, the position of the center of the test cylinder in the x–y plane of the DWB was (13.12 m, 0 m). An overview of the test cylinder is schematized in Fig. 3; Figs. 2(b and c) also show the cylinder in the DWB before filling the basin. For the second phase of the tests, a second cylinder with identical geometry was also installed with its center at (x, y) = (11.30 m, 1.6 m); the distance between the center of both cylinders was 2.42 m. This second cylinder was not instrumented and is called the dummy cylinder herein. Both cylinders were welded to a base plate (thickness of 16 mm) used to anchor them to the DWB floor.

Experimental Wave Conditions

Hurricane data in and around the Houston Ship Channel (HSC) in Texas were used to define the prototype wave conditions for this experiment. The HSC is the largest petrochemical complex in the United States with more than 4,500 ASTs and is located in a hurricane-prone region; AST failures were observed in the HSC during past major storm events. In order to determine surge and wave conditions in the HSC, numerical simulations were performed using *ADCIRC+SWAN* for Hurricane Ike, which made landfall in the Houston–Galveston region in September 2008,

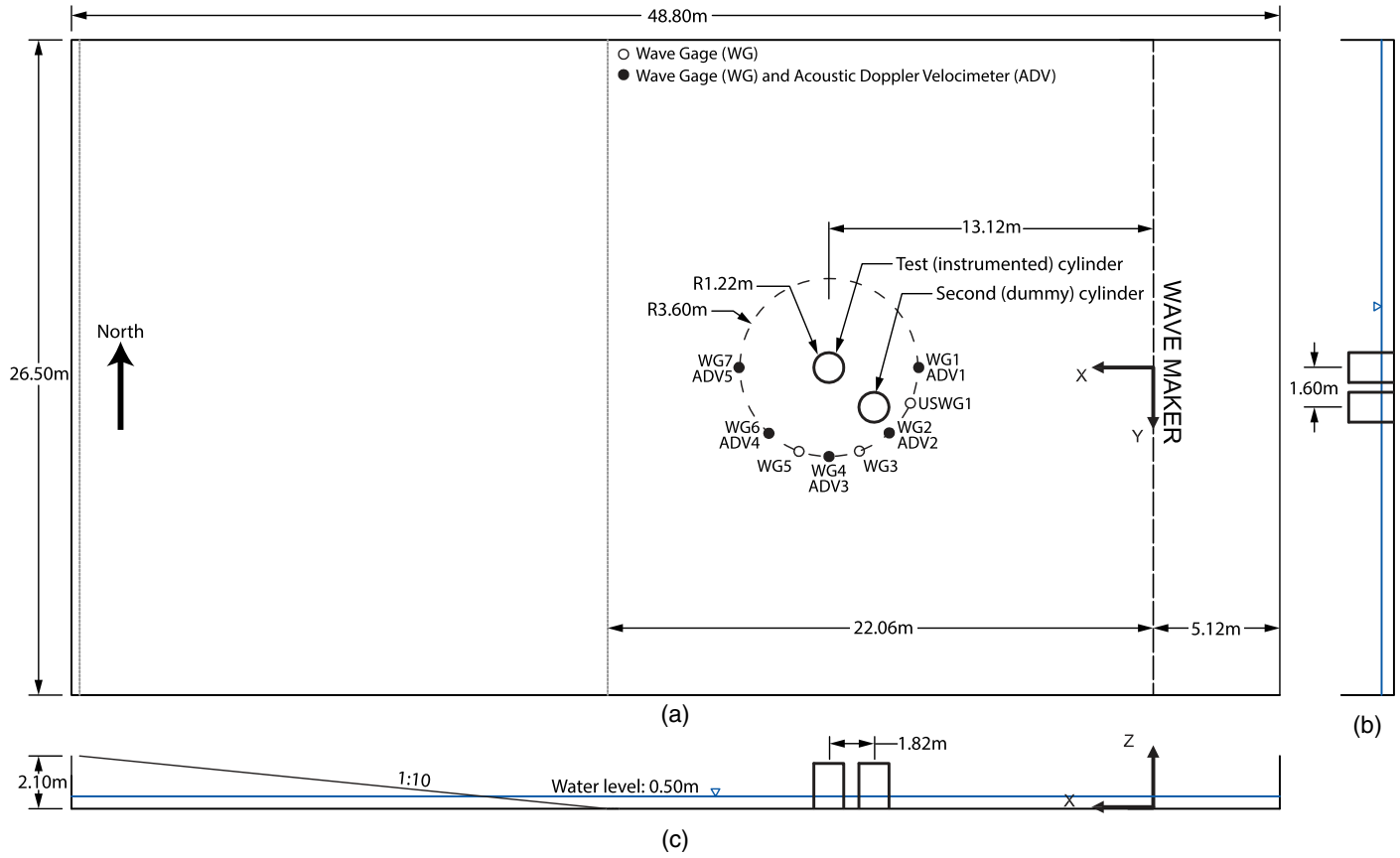

Fig. 1. General arrangement of the DWB and layout of ADVs and wave gages: (a) plan view; (b) elevation profile along the y-axis; and (c) elevation profile along the x-axis.

and for two synthetic storms developed by the Federal Emergency Management Agency (FEMA) for its Flood Insurance Study (FIS) of the Texas Coast. The two synthetic storms are commonly referred to as storms FEMA33 and FEMA36 and produce storm surge elevations with return periods of approximately 100 and 500 years in the HSC, respectively (Ebersole et al. 2016). This study mainly relied on numerical simulations to define the wave conditions due to a lack of empirical data for onshore locations such as refineries and terminals. Nonetheless, the simulation for Hurricane Ike is well validated in the literature (Hope et al. 2013), and the extracted wave parameters for all simulations were verified against empirical relations found in the USACE (2008). The typical diameters of ASTs in the HSC were also obtained from the database presented in Bernier et al. (2017a). Based on the numerical simulations and this database, the following ranges of prototype wave conditions were considered: (1) cylinder diameter: $D \geq 5$ m; (2) water depth: 2 m $\leq h \leq 7$ m; (3) peak wave period: 3.5 s $\leq T_p \leq 6$ s; and (4) significant wave height: 0.3 m $\leq H_{1/3} \leq$ 1.3 m. Such $H_{1/3}$ values can lead to wave heights (H) up to 2.0 m. Finally, from these ranges of parameters, the experimental conditions in the DWB were selected to comply with the following range of dimensionless wave conditions: (1) $0.05 \leq H/h \leq 0.65$; (2) $0.08 \leq h/L \leq 0.35$; (3) $D/L \geq 0.20$.

The different experimental conditions considered to generate the experimental dataset are summarized in Table 1; all values presented in this table are at model scale. The dimensionless parameters (H/h, h/L, and D/L) of each wave case can also be found in Table 2. Four types of waves were generated: (1) regular waves; (2) random (or irregular) waves; (3) solitary waves; and (4) double solitary waves. For all wave cases, the water depth in the DWB was kept constant at 0.5 m in order to facilitate the instrumentation. Regular waves were considered to obtain measurements under steady and repeatable wave conditions and to obtain benchmarking data for numerical models where the simulation of random waves is computationally expensive. As shown in Table 2, the regular wave cases were characterized by $0.05 \leq H/h \leq 0.65$, $0.08 \leq h/L \leq 0.32$, and $0.19 \leq D/L \leq 0.78$. At model scale, these conditions correspond to target wave heights between 0.025 and 0.325 m and target periods between 1.02 and 2.95 s. Based on the ranges of prototype wave conditions listed in the previous paragraph, the test specimen could be representative of ASTs with $4.9 \leq D \leq 17.1$ m (geometric scales between 1:4 and 1:14 under Froude Number similitude). Such large-scale experiments ensure the scalability of the measurements from model to prototype scale (Hughes 1993). It is acknowledged that in the case of flow separation or aerated water, pressure and wave runup measurements at the location of such phenomena might not be accurate at prototype scale; however, such phenomena are not expected to be significant for the wave conditions considered here. For each regular case, a total of 100 waves were generated to ensure consistent data and obtain a representative average of the experimental results. The different regular wave cases are also shown in Fig. 4, which illustrates the wave nonlinearity (H/h), shallowness (h/L), and appropriate wave theory for each case.

Random waves were considered because they represent more realistic loading conditions during a storm and can be more challenging to simulate accurately in a numerical model. The random wave cases were characterized by $0.20 \leq H_{1/3}/h \leq 0.40$, $0.08 \leq h/L_p \leq 0.33$, and $0.19 \leq D/L_p \leq 0.81$; the wavelength, L_p, was

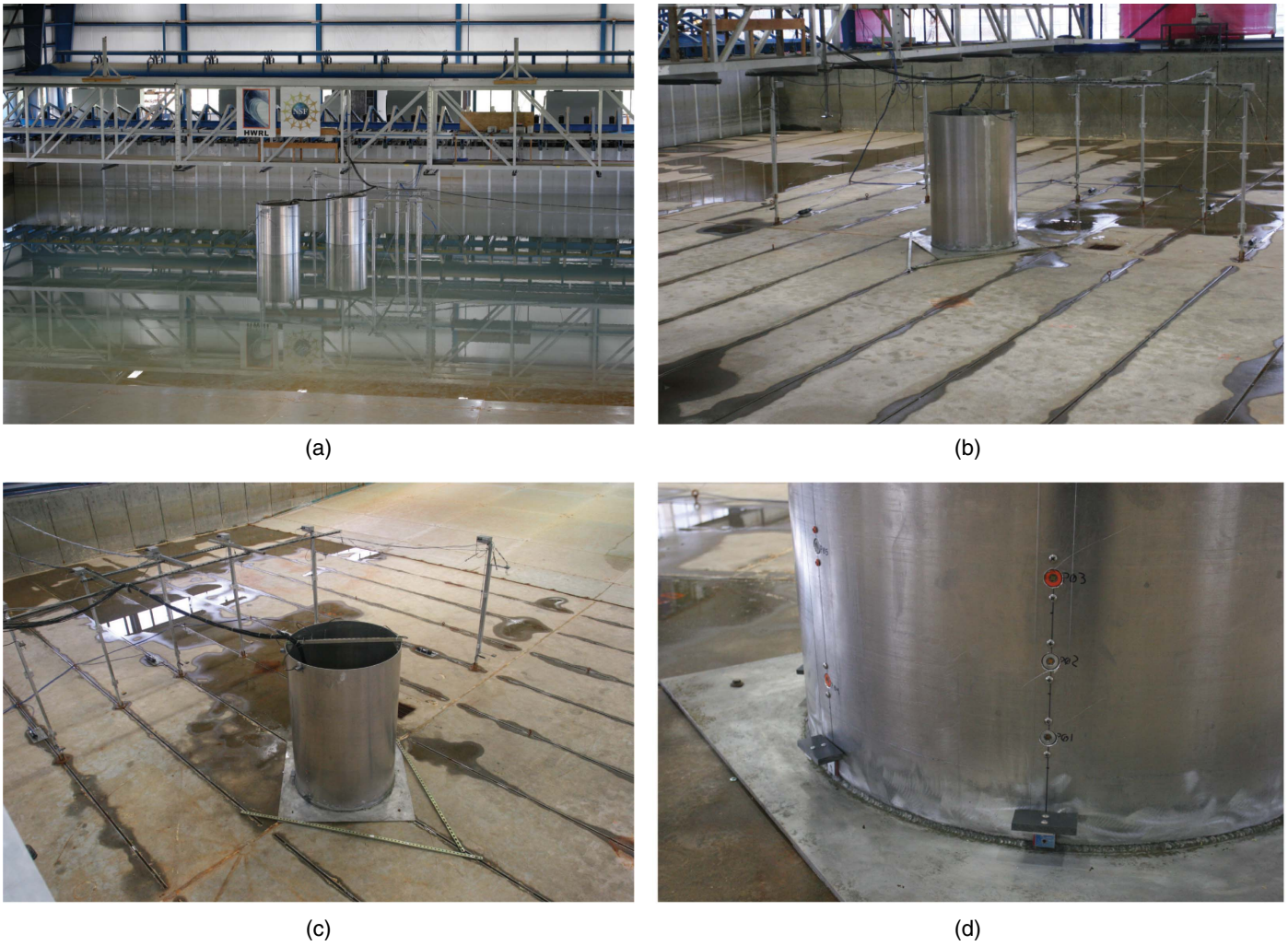

Fig. 2. Images of the experimental setup, test cylinder, and instrumentation: (a) general view of setup and wave basin; (b) rear view of test cylinder; (c) front view of test cylinder; and (d) pressure gauges and wire-resistance wave gauges. (Images by Pedro Lomonaco.)

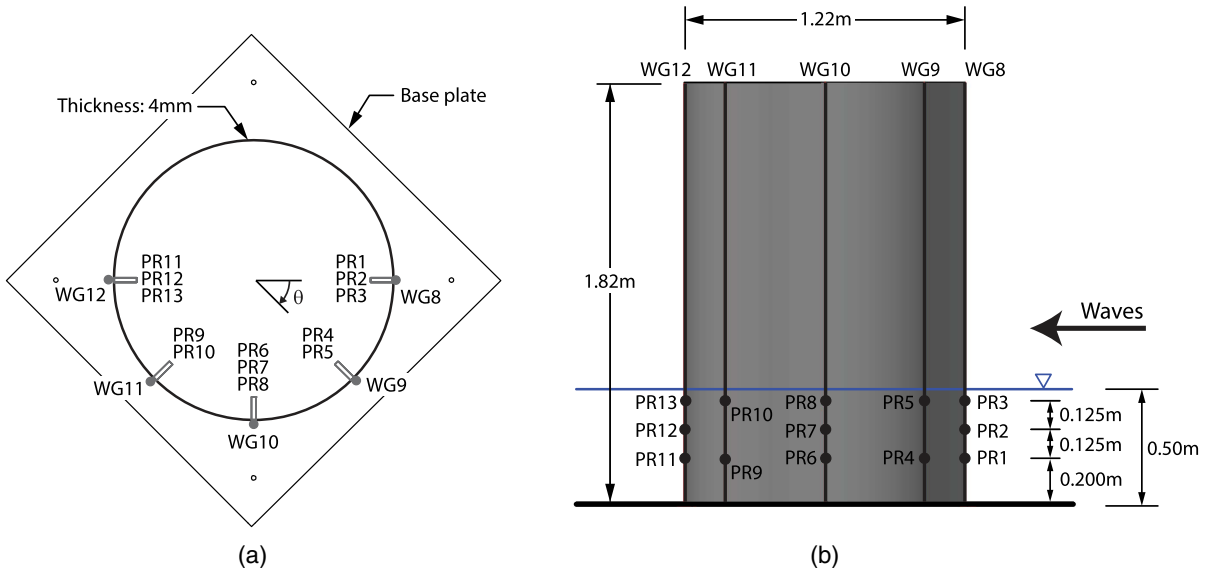

Fig. 3. Overview of the test cylinder and layout of pressure and wave runup gauges: (a) top view; and (b) side view.

Table 1. Experimental wave conditions at model scale

	Regular			Random				Solitary		Double solitary			
Case	H (m)	T (s)	h (m)	Spectrum[a]	$H_{1/3}$ (m)	T_p (s)	h (m)	H (m)	h (m)	H_a (m)	H_b (m)	λ (-)	h (m)
1	0.025	1.02	0.5	JS	0.10	1.0	0.5	0.05	0.5	0.07	0.3	0.50	0.5
2	0.100	1.02	0.5	TMA	0.10	1.0	0.5	0.10	0.5	0.07	0.3	0.75	0.5
3	0.150	1.02	0.5	JS + Spread.[b]	0.10	1.0	0.5	0.15	0.5	0.07	0.3	1.00	0.5
4	0.050	1.60	0.5	JS	0.15	1.6	0.5	0.20	0.5	—	—	—	—
5	0.150	1.60	0.5	TMA	0.15	1.6	0.5	0.25	0.5	—	—	—	—
6	0.250	1.60	0.5	JS + Spread.[b]	0.15	1.6	0.5	0.30	0.5	—	—	—	—
7	0.100	2.95	0.5	JS	0.20	3.0	0.5	0.35	0.5	—	—	—	—
8	0.200	2.95	0.5	TMA	0.20	3.0	0.5	—	—	—	—	—	—
9	0.325	2.95	0.5	JS + Spread.[b]	0.20	3.0	0.5	—	—	—	—	—	—

[a]In all cases, the wave spectrum is defined with $\gamma = 3.3$.
[b]The spreading parameter is $s = 16$.

Table 2. Experimental wave conditions in dimensionless form

	Regular			Random			Solitary			Double solitary	
Case	H/h	h/L	D/L	$H_{1/3}/h$	h/L_p[a]	D/L_p[a]	H/h	h/L[b]	D/L[b]	H_a/h	H_b/h
1	0.05	0.32	0.78	0.20	0.33	0.81	0.10	0.05	0.11	0.14	0.60
2	0.20	0.32	0.78	0.20	0.33	0.81	0.20	0.06	0.16	0.14	0.60
3	0.30	0.32	0.78	0.20	0.33	0.81	0.30	0.08	0.19	0.14	0.60
4	0.10	0.16	0.40	0.30	0.16	0.40	0.40	0.09	0.22	—	—
5	0.30	0.16	0.40	0.30	0.16	0.40	0.50	0.10	0.25	—	—
6	0.50	0.16	0.40	0.30	0.16	0.40	0.60	0.11	0.27	—	—
7	0.20	0.08	0.19	0.40	0.08	0.19	0.70	0.12	0.30	—	—
8	0.40	0.08	0.19	0.40	0.08	0.19	—	—	—	—	—
9	0.65	0.08	0.19	0.40	0.08	0.19	—	—	—	—	—

[a]For the random wave cases, L_p was computed using h and T_p.
[b]For the solitary wave cases, $L = 2\cosh^{-1}(10)/k$, where $k = \sqrt{3H/4h^3}$.

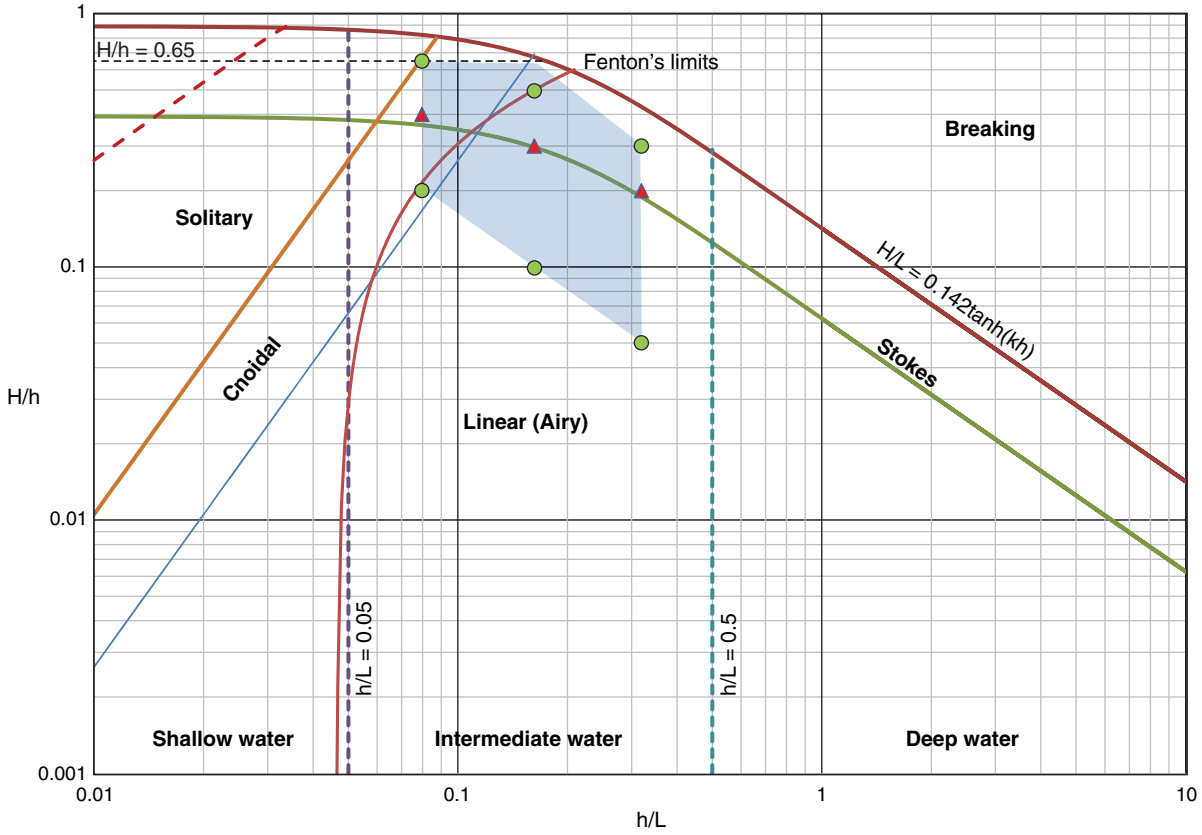

Fig. 4. Experimental wave conditions (H/h versus h/L). The shaded area represents the range of the target experimental wave conditions. Each circle represents a regular wave case while each triangle represents a regular and random case.

computed using h and T_p. At model scale, this corresponds to target significant wave heights between 0.1 and 0.2 m and peak periods between 1.0 and 3.0 s. As shown in Fig. 4, only three combinations of wave parameters were considered. However, three types of wave spectra were considered for each combination: (1) the JONSWAP (JS) spectrum; (2) the TMA (Texel-MARSEN-ARSLOE) spectrum, which is a modification of the JONSWAP spectrum to take into account the water depth; and (3) the JONSWAP spectrum with directional spreading defined using the Longuet-Higgins cosine-power spreading function (USACE 2008). The spectrum peak shape factor was fixed at $\gamma = 3.3$ for all random wave cases, while the controlling parameter of the Longuet-Higgins cosine-power spreading function was fixed at $s = 16$ for random wave cases 3, 6, and 9. Approximately 500 waves were generated for each random wave case to obtain representative wave statistics.

Solitary waves were also considered for additional benchmarking. Solitary waves are applicable in the case of tsunami and are also a way to understand the effect of very long, nonlinear waves as they could be expected for waves propagating over flooded land. Seven cases with wave heights between 0.05 and 0.35 m were generated ($0.10 \le H/h \le 0.70$). The double solitary waves were not initially designed and generated for this project. However, they were included in the dataset because they can be useful for future studies where wave-wave interaction is examined. The three double solitary wave cases were characterized by a first wave height (H_a) of 0.07 m, second wave height (H_b) of 0.3 m, and time lag coefficient (λ) varying between 0.5 and 1.0; the time lag between the two solitary waves was defined as λT_f, where T_f is the time required to generate the first solitary wave (Altomare et al. 2017).

Instrumentation and Data Acquisition

In order to generate benchmarking data, the instrumentation was designed to measure wave runups and pressures on the test cylinder [i.e., the cylinder with center located at $(x, y) = (13.2\ \text{m}, 0\ \text{m})$] as well as water surface elevations and velocities around the test cylinder. Table 3 provides the description, nomenclature, and coordinates of all instruments installed for the experiment. The water surface elevations around the test cylinder were measured using seven wire-resistance wave gauges (WGs 1–7, ImTech Inc.) and one ultrasonic wave gauge (USWG 1, Senix Corp.). As shown in Fig. 1(a), the wave gauges were arranged in a semi-circle with a radius of 3.6 m and center at $(x, y) = (13.2\ \text{m}, 0\ \text{m})$. The wave gauge setup is shown in the photos presented in Figs. 2(a and b). Five acoustic-Doppler velocimeters (ADVs 1–5, Nortek Vectrino) were also installed on the semi-circle setup to measure water-particle velocity. The five ADVs were colocated with WGs 1, 2, 4, and 7. To ensure the quality of the ADV measurements, seeding was added to the DWB (Spherical Hollow Glass Spheres D90-100 microns). To obtain an adequate resolution of the dynamic pressure distribution, 13 pressure gauges (PRs 1–13, GE/Druck Inc. PDCR 830) were installed on one-half of the test cylinder. As shown in Fig. 3, the pressure gauges were arranged into five vertical arrays spaced by arcs of 45°. With respect to the cylinder

Table 3. Instrument description, nomenclature, and location

Instrument description	Instrument	x (m)	y (m)	z (m)
Wavemaker displacement	WMDISP15	—	−0.460	—
Wavemaker wave gauge	WMWG15	—	0.000	—
Wavemaker trigger signal	WMSTART	—	—	—
Ultrasonic wave gauge	USWG1	9.768	1.371	1.571
Resistive wave gauge	WG1	9.481	0.007	—
Resistive wave gauge	WG2	10.706	2.689	—
Resistive wave gauge	WG3	11.910	3.429	—
Resistive wave gauge	WG4	13.140	3.621	—
Resistive wave gauge	WG5	14.347	3.413	—
Resistive wave gauge	WG6	15.569	2.692	—
Resistive wave gauge	WG7	16.777	−0.006	—
Resistive wave gauge (runup)	WG8	12.575	−0.089	—
Resistive wave gauge (runup)	WG9	12.713	0.363	—
Resistive wave gauge (runup)	WG10	13.127	0.588	—
Resistive wave gauge (runup)	WG11	13.564	0.410	—
Resistive wave gauge (runup)	WG12	13.747	−0.038	—
Pressure gauge	PR1	12.585	−0.081	0.216
Pressure gauge	PR2	12.585	−0.084	0.340
Pressure gauge	PR3	12.585	−0.081	0.467
Pressure gauge	PR4	12.725	0.359	0.216
Pressure gauge	PR5	12.723	0.358	0.467
Pressure gauge	PR6	13.125	0.575	0.214
Pressure gauge	PR7	13.128	0.575	0.340
Pressure gauge	PR8	13.128	0.576	0.465
Pressure gauge	PR9	13.558	0.395	0.216
Pressure gauge	PR10	13.558	0.397	0.466
Pressure gauge	PR11	13.732	−0.042	0.219
Pressure gauge	PR12	13.732	−0.045	0.339
Pressure gauge	PR13	13.734	−0.044	0.466
Acoustic-Doppler velocimeter	ADV1	9.472	0.019	0.253
Acoustic-Doppler velocimeter	ADV2	10.699	2.704	0.253
Acoustic-Doppler velocimeter	ADV3	13.137	3.652	0.252
Acoustic-Doppler velocimeter	ADV4	15.571	2.728	0.253
Acoustic-Doppler velocimeter	ADV5	16.786	0.033	0.250

base plate, five pressure gauges were located at $z = 0.2$ m ($z/h = 0.4$), three were located at $z = 0.32$ m ($z/h = 0.65$), and five were located at $z = 0.45$ m ($z/h = 0.9$). The wave runup was measured by using five wire-resistance wave gauges (WGs 8–12, ImTech Inc.) located on the same vertical axis as the pressure gauges. Fig. 2(d) shows a photo of the pressure gauges and wave gauges on the test cylinder. Finally, the two first instruments shown in Table 2 measured the displacement (WMDISP15) and the water surface elevation (WMWG15) at the 15th actuator and 15th paddle of the wavemaker, respectively. At the exception of the directional wave cases (random wave cases 3, 6, and 9), the displacements and water surface elevations of the other actuators and paddles should be identical. A trigger signal (WMSTART) was also measured to determine when the wavemaker started and stopped moving.

During each experimental trial, all instruments were synchronized and data were recorded using two real-time data acquisition systems (National Instruments PXI-8109 and PXI-8119), one for the ADVs and one for all other instruments. The sampling rate was fixed at 100 Hz for all instruments, while the sampling duration was a function of the wave case and the total number of generated waves. The sampling duration varied between 300 and 480 s for the regular wave cases and between 660 and 1,680 s for the random wave cases, and it was fixed at 180 s for the solitary and double solitary wave cases. The sampling durations captured 30–35 s of still water, wave ramp up, full propagation of a sufficient number of waves, wave ramp down, and an additional 60–100 s for the wave basin to return to relatively calm conditions once the wavemaker stopped. Between each trial, there was an additional 10–15 min waiting period, which was not recorded, to ensure that the water conditions in the DWB returned to a completely still and calm state.

Experimental Plan and Process

The experiments were performed in four phases summarized in Table 4. All experimental phases were completed within a time frame of approximately 3 weeks. The first phase consisted of the regular, random, and solitary wave cases shown in Table 1 with only the test cylinder in the DWB. At the end of phase 1, an amplifier was replaced to resolve issues with drifting wave runup gauges (WGs 8–12) and improve the quality of these measurements. Also, the configuration of the ADVs was modified to increase the velocity range as saturation was observed during the two last wave trials of phase 1 (solitary wave cases 6 and 7). During phase 2, both the test and the dummy cylinders were installed in the DWB to investigate the interferences produced by the dummy cylinder on the test cylinder and to provide additional benchmarking data. The double solitary wave cases were also introduced during this experimental phase. The location of the dummy cylinder was constrained by the instrumentation and was based on observations of AST layouts in refineries and terminals along the HSC; the distance between the outer shells of each cylinder (B) was approximately equal to the cylinders' diameter (D). Phase 3 consisted of replicating phase 1 to obtain the wave runup and velocity measurements without drifting or saturation issues. Phase 3 also included the double solitary wave cases with a single cylinder. Lastly, phase 4 consisted of performing all the wave cases without any cylinder in the DWB. Such tests, also known as undisturbed wave tests, are useful to validate wave generation and propagation in numerical models without the presence of a structure.

Table 4. Experiment phases summary

Phase	Wave conditions	Description
1	Regular, random, solitary	With test cylinder only
2	Regular, random, solitary, double solit.	With both test and dummy cylinders
3	Regular, random, solitary, double solit.	With test cylinder only—Wave runup gauges
4	Regular, random, solitary, double solit.	Without any cylinder—Undisturbed conditions

Data Processing and Curation

Data from all wave trials and experimental phases were curated and published using the NHERI DesignSafe.CI web-based platform; DesignSafe.CI provides a platform for data management, analysis and publication, including tools that facilitate organizing, categorizing, and describing the data. This project was among the first to serve as a test case for the DesignSafe.CI curation and publication pipeline. The experimental dataset can be publicly accessed and downloaded using the following Digital Object Identifier (DOI): 10.17603/DS27D4G (Bernier et al. 2017b); the overall size of the dataset is approximately 14 GB. Fig. 5 illustrates the organization of the experimental data in DesignSafe.CI. For each of the three configurations of the DWB (i.e., no cylinder, one cylinder, and two

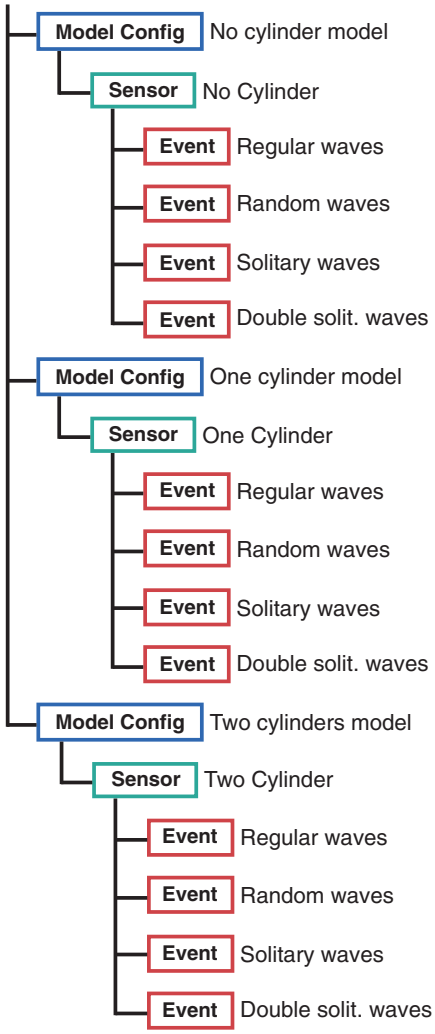

Fig. 5. Experimental tree for data curation in DesignSafe.CI.

cylinders), the data was divided into four events corresponding to each type of wave; data from phases 1 and 3 of the experiment were grouped together under the one cylinder configuration. Each event directory contains the raw data (binary and ASCII formats for ADVs and ASCII format for other instruments), intermediate data (ASCII format), photos (JPEG format), videos (MPEG format), and log files (PDF format). The raw and intermediate data were further organized into directories for each wave trial. The trial numbers in DesignSafe.CI do not necessarily correspond to the wave cases presented in Table 1 as some wave cases were repeated due to incorrect sampling duration; the original trials were retained and published to preserve the integrity of the dataset. As a result, users should refer to the log files located in each event directory to navigate through the dataset and identify the wave conditions of each trial. All raw and intermediate data ASCII files also include headers providing metadata such as the wave conditions; timestamp; data acquisition system, channels, and sampling details; calibration data; and configuration, signal-to-noise ratio, and correlation of the measurements for the ADVs. Finally, as shown in Fig. 5, each event directory is linked to a model configuration and sensor information directories. The model configuration directory provides the wavemaker input files (binary and ASCII formats), photos, and layouts of the DWB configuration (PDF and DWG formats) for the event. The sensor information directory provides the calibration data (Excel format), wiring details (Excel format), sensor photos, and instrument locations (Excel format) for the event.

The raw data published on DesignSafe.CI correspond to the data directly recorded by the acquisition system without any modification, while the intermediate data correspond to post-processed data. The post-processing consisted of the application of calibrations to convert the raw data into engineering units, zeroing of the wave gauges, cleanup of the data, and properly orienting the ADV data with respect to the DWB coordinate system. The calibration data were obtained by draining and refilling the DWB. Because the experiment occurred over a relatively long period of time, the calibration data were updated frequently (approximately once or twice a week). The zero datum of the wave gauges was fixed at the still water elevation prior to any motions of the wavemaker. The data of all instruments were also clipped using the trigger signal (WMSTART) to remove unnecessary portions at the beginning and end of the signal when the wavemaker was stopped. Finally, the ultrasonic wave gauge and the ADVs data were despiked and cleaned up using the procedure presented in Baldock et al. (2009) to remove outliers, signal dropouts, and poor-quality data. Any additional post-processing, such as drift correction for the wave runup gauges of phase 1 or additional filtering, is left to the user of the dataset.

Experimental Data

Experimental Time Series and Qualitative Observations

One of the main objectives of this experiment was to obtain an experimental dataset for the validation of numerical models of large cylindrical structures such as ASTs subjected to waves. This section presents samples of the experimental data to demonstrate the quality of the measurements for numerical benchmarking and provide qualitative observations crucial to understanding and using the data. Fig. 6 shows a snapshot of the time series of selected sensors from regular and random wave cases 5 and phase 1 of the experiment. Figs. 6(a and e) show the water surface elevations at

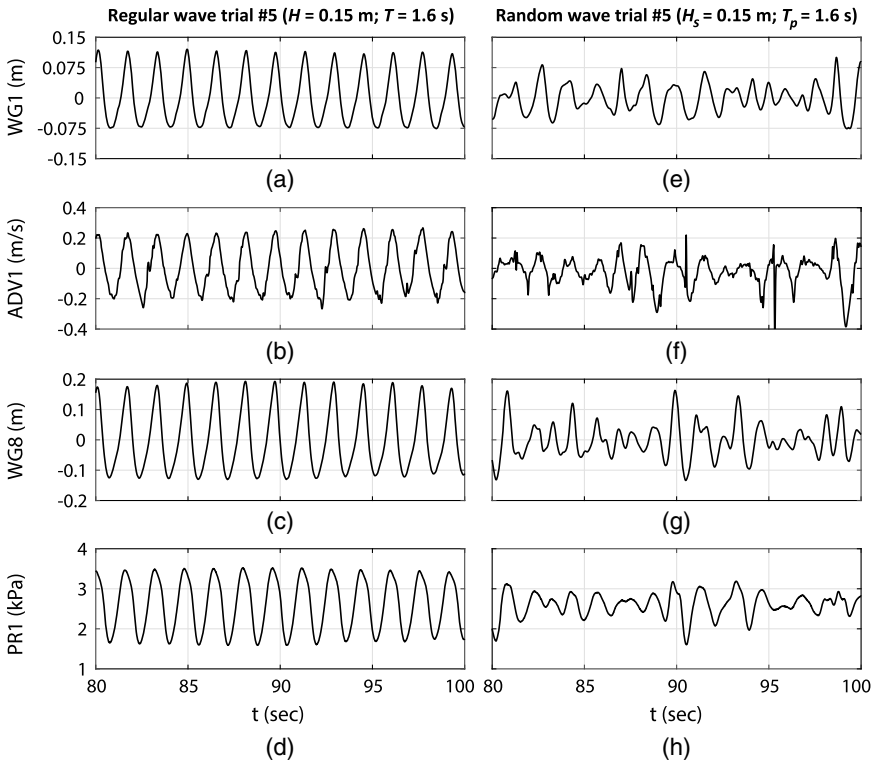

Fig. 6. Snapshot (20 s) of experimental time series from regular and random wave cases 5 and phase 3. Regular wave case 5: (a) water surface elevations at WG1; (b) water velocities at ADV1; (c) wave runups at WG8; and (d) pressures at PR1. Random wave case 5: (e) water surface elevations at WG1; (f) water velocities at ADV1; (g) wave runups at WG8; and (h) pressures at PR1.

J. Struct. Eng., 2020, 146(5): 04720001

WG1 on the upwave side of the test cylinder and at y = 0 m. Figs. 6(b and f) show the horizontal (x-axis) particle velocities measured by ADV1 at the same location. Figs. 6(c and g) show the wave runups measured by WG8 on the upwave surface of the test cylinder at $y = 0$ m. Lastly, Figs. 6(d and h) show the pressures measured by PR1 at $(y, z) = (0\text{ m}, 0.216\text{ m})$ on the upwave surface of the test cylinder. Overall, the observations of experimental time series indicate that the instruments and the adopted sampling rate of 100 Hz can resolve the pressures, water surface elevations, wave runups, and velocities around the test cylinder for the selected experimental wave conditions. As expected, the ADV signals were generally noisier than the other instruments. Nonetheless, the ADV measurements still provide a good estimation of water velocities for the validation and benchmarking of numerical models.

To better understand how waves propagated in the DWB and affected measurements when repeatable wave conditions were generated, a full-time series of water surface elevations is presented in Fig. 7. This figure shows that the water surface elevation was still at first. Then, the wavemaker ramped up for 20 s, and waves started propagating. Waves hit the sloped beach at the end of the DWB, and a small fraction of energy reflected. Waves also reflected from the cylinder(s), producing a concentric pattern of waves. Radiating waves then interacted with the incoming waves and also reflected from the lateral walls and the wavemaker. In addition, with two cylinders in the DWB, the radiating waves coming from one cylinder would interact with the other cylinder, creating another radiating pattern that would then interact with the first cylinder, and so on. This complex multidirectional interference developed over time before reaching a quasi-steady state and measurements becoming stable. The term quasi-steady is employed here because more energy was continuously introduced in the DWB than dissipated and because other sources of variability such as random effects, turbulence, and instrument uncertainty were also present. This phenomenon is observed in Fig. 7, which shows that it took approximately 80 s to reach a quasi-steady state. As discussed in the next section, depending on the wave conditions, instrument location, and number of cylinders in the DWB, the interference can produce constructive or destructive interactions and thereby either increase or reduce the water surface elevation, velocity, pressure, or runup. When analyzing the data, the time frame should be limited to the quasi-steady portion of the signal to ensure the interference

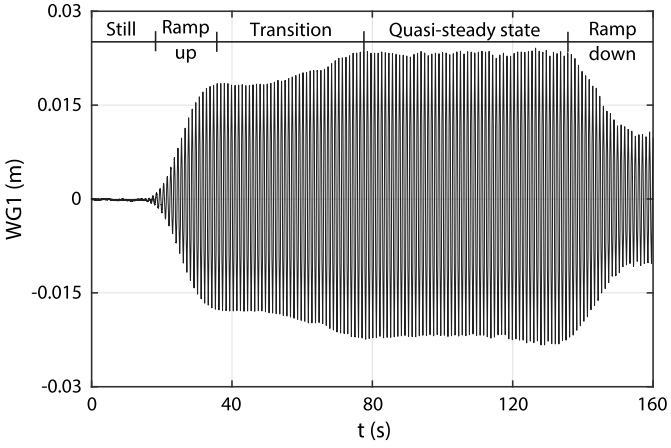

Fig. 7. Time series of water surface elevations at WG1 from regular wave case 1 and phase 2.

effects are developed and to avoid considering variability that is intrinsic to the experimental setup.

Effects of the Second Cylinder

To further demonstrate the usefulness and quality of the experimental data, this section presents the interference created by the dummy cylinder on the test cylinder. The dummy cylinder was described previous, and its location is shown in Fig. 1; the relative distance between both cylinders (B/L) was approximately equal to the relative diameter of the cylinders (D/L). For conciseness, experimental results are presented only for regular wave cases. Before proceeding to the comparison between the measurements from the different experimental phases, the repeatability of the wavemaker motion (WMDISP15) was first assessed to ensure that the wave inputs were consistent across the experimental phases for a given wave case. Differences less than 0.1% were observed in the wavemaker motion between the different experimental phases. Because the water depth was kept constant at 0.5 m (±0.2 mm) during the experiment, for a given wave case, any significant perturbations in the measurements between the different experimental phases can be assumed to be because of the presence of the test or the dummy cylinders in the DWB and the interference created by them.

The interference created by the dummy cylinder is presented in Figs. 8 and 9 for regular wave cases 1, 3, 4, 6, 7, and 9; all data were obtained from phases 2, 3, and 4. Fig. 8 shows the interference effects on the measurements around the test cylinder [mean wave height ($\bar{H}$) and mean peak horizontal particle velocity ($\bar{u}_{\max}$)], while Fig. 9 shows the effects on the test cylinder [mean runup ($\bar{R}_u$) and mean peak dynamic pressure ($\bar{P}_{\max}$)]. In these figures, θ is the angle between the x-axis and a line joining the center of the test cylinder and the (x, y) position of each instrument; $\theta = 0°$ is on the upwave side of the test cylinder [Fig. 3(a)]. In the case of dynamic pressure, the experimental results are also compared with the analytical solutions proposed by MacCamy and Fuchs (1954) and Linton and Evans (1990) for one and two cylinders, respectively. Experimental results were normalized by using the undisturbed wave height ($\langle H \rangle$), or a function thereof, for each wave case. The undisturbed wave height was computed by averaging the wave heights from the eight wave gauges (WGs 1–7 and USWG1) in the DWB during phase 4. The undisturbed wave heights used to normalize the experimental data are shown in Table 5. As discussed in the previous section, to obtain the mean measured values presented in Figs. 8 and 9, only the portion of the signals that could be considered as quasi-steady was analyzed. The number of generated waves (100) was generally sufficient to adequately capture the quasi-steady state and obtain a representative average of the measurements. To display the fidelity of the measurements, the standard errors for each of the mean measured values are also presented in Figs. 8 and 9; the relative standard error was generally less than 5% for most instruments, while it could reach up to 10% for the ADVs.

The upper panel of Fig. 8 presents the effects on the normalized wave heights ($\bar{H}/\langle H \rangle$) of introducing the test and dummy cylinders in the DWB. Figs. 8(a–f) and Table 5 indicate consistent measurements across the eight wave gauges when no cylinder was in the DWB. However, as shown in Fig. 8, the interference created by the test cylinder significantly perturbed the wave field in the DWB. Introducing the dummy cylinder further amplified the perturbation of the wave field around the test cylinder. For the wave cases with $D/L = 0.78$ [Figs. 8(a and d)], the wave height significantly increased in the front and on the side of the test cylinder ($\theta = 0°$ and $\theta = 90°$), while the wave height generally decreased for other wave

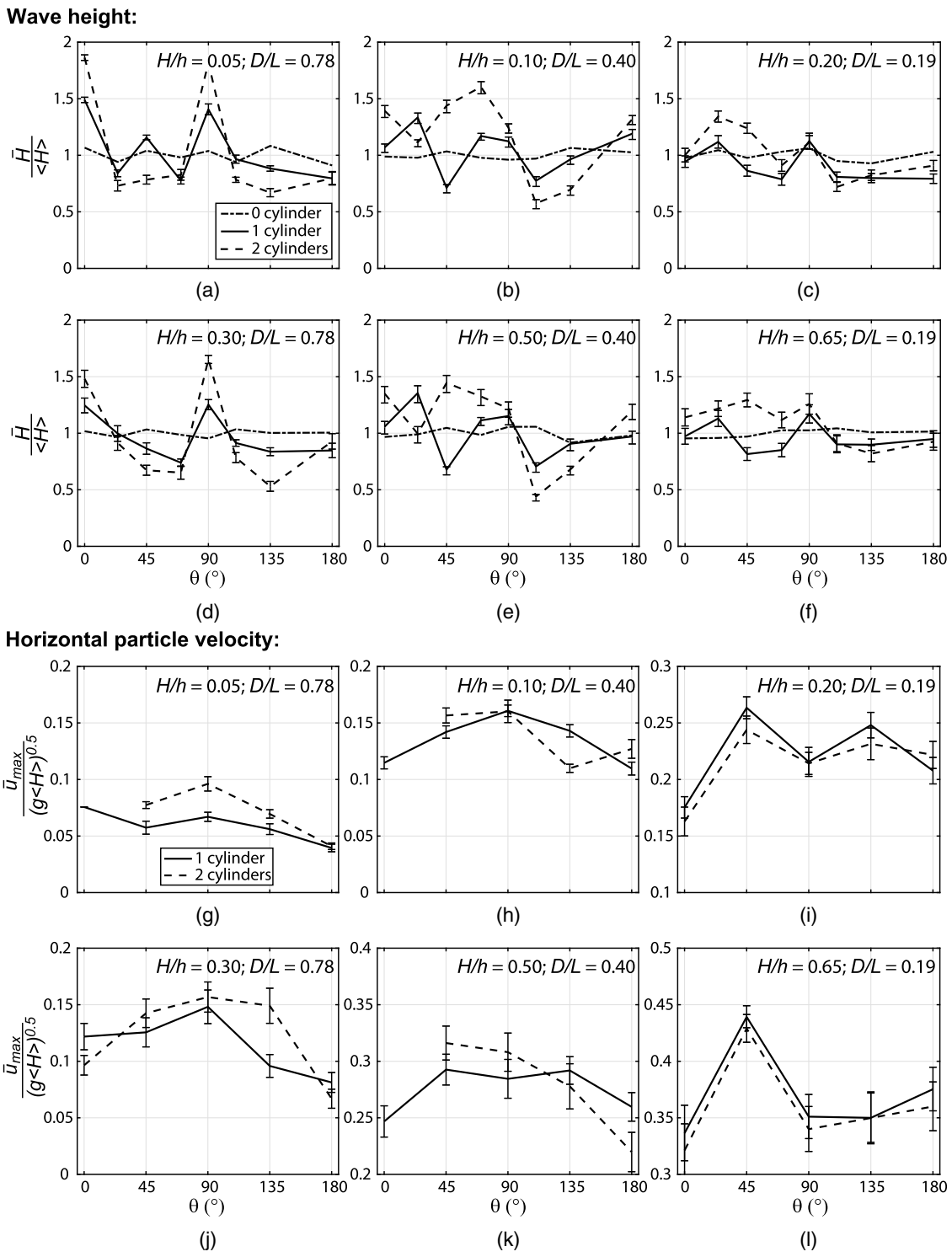

Fig. 8. Wave heights and water velocities for regular wave cases. Normalized wave heights: (a) case 1; (b) case 4; (c) case 7; (d) case 3; (e) case 6; and (f) case 9. Normalized horizontal particle velocities: (g) case 1; (h) case 4; (i) case 7; (j) case 3; (k) case 6; and (l) case 9. Data were obtained from phases 2, 3, and 4. The vertical bars represent the standard error of the mean measurements.

gauge locations compared to the case with no cylinder. For decreasing values of D/L, the interference effects created by both the test and the dummy cylinders became less significant, as observed in Figs. 8(c and f). A similar trend is also observed in the lower panel of Fig. 8 for the normalized horizontal particle velocities ($\bar{u}_{\max}/(g\langle H\rangle)^{0.5}$), where the effects of the dummy cylinder on the water velocity became less significant as the relative diameter of the cylinders and the relative distance between the cylinders ($B/L \approx D/L$) decreased.

The perturbation of the wave field created by the presence of the dummy cylinder also affected the runup and dynamic pressure acting on the test cylinder, as shown in Fig. 9. The upper panel of Fig. 9 shows the effects of the dummy cylinder on the normalized wave runups ($\bar{R}_u/\langle H\rangle$), while the lower panel shows the effects on

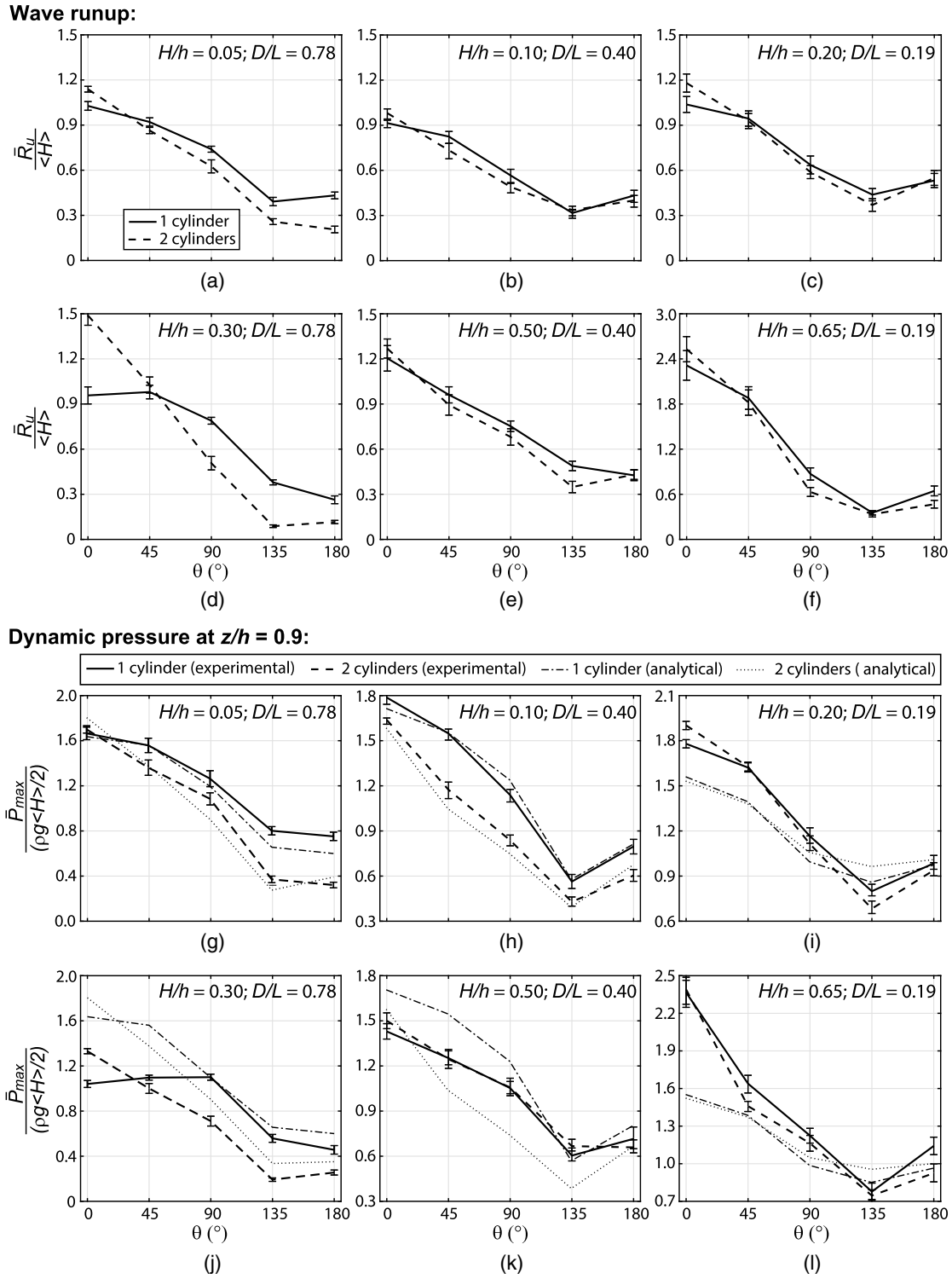

Fig. 9. Wave runups and dynamic pressures for regular wave cases. Normalized runups: (a) case 1; (b) case 4; (c) case 7; (d) case 3; (e) case 6; and (f) case 9. Normalized dynamic pressures at $z/h = 0.9$: (g) case 1; (h) case 4; (i) case 7; (j) case 3; (k) case 6; and (l) case 9. Data were obtained from phases 2 and 3. The vertical bars represent the standard error of the mean measurements.

the normalized dynamic pressures ($\bar{P}_{\max}/(\rho g\langle H\rangle/2)$). The effects on the pressure are only shown for $z/h = 0.9$, but similar results were observed for the other pressure gauge elevations. Figs. 9(a–f) show that the additional interference created by the dummy cylinder amplified the wave runup on the upwave face of the test cylinder ($\theta < 30°$–$45°$), while it decreased the runup on the side and downwave faces of the cylinder ($\theta > 30°$–$45°$). Consequently, the dynamic pressure was also generally increased on the upwave face of the test cylinder and decreased on the downwave face, as illustrated in Figs. 9(g–l). Following the same trend as the wave field measurements, the perturbations of the runup and dynamic pressure generally became more significant as D/L and B/L increased.

Table 5. Wave heights used to normalize the experimental data

Case	WG1 (m)	USWG1 (m)	WG2 (m)	WG3 (m)	WG4 (m)	WG5 (m)	WG6 (m)	WG7 (m)	$\langle H \rangle$ (m)	*STD* (m)
Reg 1	0.026	0.023	0.025	0.024	0.025	0.023	0.026	0.022	0.024	0.002
Reg 3	0.137	0.130	0.139	0.133	0.129	0.140	0.135	0.136	0.135	0.004
Reg 4	0.051	0.051	0.053	0.051	0.050	0.050	0.055	0.053	0.052	0.002
Reg 6	0.204	0.209	0.221	0.208	0.223	0.223	0.193	0.207	0.211	0.011
Reg 7	0.109	0.117	0.109	0.115	0.119	0.106	0.104	0.115	0.112	0.005
Reg 9	0.278	0.280	0.283	0.299	0.299	0.304	0.294	0.296	0.292	0.010

Note: $\langle H \rangle$ = ensemble average of the eight wave gauges of phase 4 and *STD* = standard deviation. *Reg* = regular wave case.

For example, on the downwave face of the test cylinder, the reductions were between 5% and 55% for the wave runup, and between 10% and 65% for the pressure for $D/L = 0.78$. Whereas for $D/L = 0.19$, they were only between 0% and 25% for the runup and between 0% and 20% for the pressure. Moreover, for $D/L = 0.78$, increasing the wave height significantly amplified the runup and pressure at $\theta = 0°$; for $H/h = 0.05$, the increase of the runup and pressure were 10% and 2%, respectively, while they were 65% and 30% for $H/h = 0.30$, respectively. However, no similar trend for the wave height was observed for the two other relative diameters. As expected, for the linear wave cases shown in Figs. 9(g and h), analytical solutions are in good agreement with the experimental pressure measurements, providing a sanity check of the quality of the data; differences less than 10% are observed on the upwave face of the test cylinder, while larger differences can be observed on the downwave face due to wave reflection in the DWB. However, for the nonlinear wave cases shown in Figs. 9(i–l), significant differences are observed between the analytical and experimental results. These differences can reach up to 55% on the upwave face of the cylinder, highlighting the relevance of the experimental dataset to develop and validate numerical models to adequately estimate wave loads on large-scale cylinders.

Overall, the results presented in Figs. 8 and 9 indicate that the interference created by the dummy cylinder significantly affected the wave loads on the test cylinder, highlighting the potential importance of considering adjacent cylinders or structures when estimating wave loads on a specific large-scale cylindrical structure such as an AST. The location of the cylinders tested in this experiment is only one out of an almost-infinite number of possible configurations. Thus, future numerical work and potential additional experimental work are required to further understand how wave loads are affected by the relative location and the presence of multiple large-scale cylinders such as ASTs during storm surge events. The experimental dataset assembled and presented here provides useful benchmarking data to support such future numerical studies.

Discussion and Conclusions

This paper presented an overview of laboratory experiments of large-scale cylinders representative of ASTs subjected to waves. The experiments aimed to develop a comprehensive dataset of water surface elevations, water velocities, pressures, and wave runups for numerical benchmarking and investigate the interference created by a dummy cylinder placed in front of an instrumented cylinder. The experiments were conducted in the DWB at Oregon State University. To generate the experimental dataset, more than 100 regular, random, solitary, or double solitary wave cases were conducted, covering the range of wave conditions that could be encountered by ASTs during storm surge events. The experiments were performed in four distinct phases to obtain measurements with a single cylinder, two cylinders, and no cylinders in the DWB. The experimental dataset was stored, curated, and published in an open access repository using DesignSafe.CI and also served to test and improve the data curation pipeline in DesignSafe.CI.

An initial analysis of the experimental data illustrated the quality and relevance of the measurements for numerical benchmarking. The experiments performed as part of this study constitute an essential source of data to enable a better understanding of the structural behavior of ASTs during hurricane events and facilitate the development of accurate and reliable numerical models to reflect loads on ASTs during storm surge events. Work is currently underway to use and further analyze this dataset to develop novel fluid-structure interaction numerical models of ASTs subjected to multi-hazard storm events and to further investigate interference and shielding effects within a petrochemical complex. Future experimental work could focus on larger-scale cylinders and more complex layouts of these cylinders to provide a richer experimental dataset as well as move beyond the nondestructive testing conducted herein to capture the structural behavior of ASTs subjected to storm surge and wave loads.

Data Availability Statement

Some or all data, models, or code generated or used during the study are available in a repository or online in accordance with funder data retention policies (Large-scale laboratory experiments of wave impacts on vertical cylinders, DesignSafe-CI, https://doi.org/10.17603/DS27D4G).

Acknowledgments

This material is based upon work supported by the Hinsdale Wave Research Laboratory, which is a major facility funded by the National Science Foundation (award number CMMI-1519679). The authors also acknowledge the partial support of this research by the National Science Foundation under awards CMMI-1635784 and CMMI-1635115. The contributions of the first author were also supported in part by the Natural Sciences and Engineering Research Council of Canada. The authors thank Tim Maddux, Bret Bosma, and the HRWL staff for their contribution to the experimental setup and testing, as well as Maria Esteva, Josue Balandrano Coronel, Ammar Musa, and Olajide Ogunmola for their help with the data curation in DesignSafe.CI. Any opinions, findings, and conclusions or recommendations expressed in this paper are those of the authors and do not necessarily reflect the views of the sponsors.

References

Akyildiz, H. 1999. "The theoretical and experimental study of the nonlinear wave forces acting on a rigid body in water of finite depth." Ph.D. thesis, Dept. of Shipbuilding and Ocean Engineering, Istanbul Technical Univ.

Akyildiz, H. 2002. "Experimental investigation of pressure distribution on a cylinder due to the wave diffraction in a finite water depth." *Ocean Eng.* 29 (9): 1119–1132. https://doi.org/10.1016/S0029-8018(01)00061-0.

Altomare, C., P. Lomonaco, J. Gonzalez-Cao, J. M. Dominguez, A. J. C. Crespo, and M. Gomez-Gesteria. 2017. "Generation of trains of tsunami-like solitary waves in DualSPHysics model." In *Proc., 12th Int. SPHERIC Workshop*. Vigo, Spain: Universidade de Vigo.

Baldock, T. E., D. Cox, T. Maddux, J. Killian, and L. Fayler. 2009. "Kinematics of breaking tsunami wavefronts: A data set from large scale laboratory experiments." *Coastal Eng.* 56 (5–6): 506–516. https://doi.org/10.1016/j.coastaleng.2008.10.011.

Bernier, C., J. R. Elliott, J. E. Padgett, F. Kellerman, and P. B. Bedient. 2017a. "Evolution of social vulnerability and risks of chemical spills during storm surge along the Houston ship channel." *Nat. Hazard. Rev.* 18 (4): 04017013. https://doi.org/10.1061/(ASCE)NH.1527-6996.0000252.

Bernier, C., Y. Lin, J. E. Padgett, C. Dawson, P. Lomonaco, and D. Cox. 2017b. "Large-scale laboratory experiments of wave impacts on vertical cylinders." DesignSafe-CI. Experiments dataset. Accessed September 27, 2017. https://www.designsafe-ci.org/data/browser/public/designsafe.storage.published//PRJ-1293.

Chakrabarti, S. K., A. R. Libby, and D. J. Kompare. 1986. "Dynamic pressures around a vertical cylinder in waves." In *Proc., 18th Annual Offshore Technology Conf.*, 193–196. Houston: Offshore Technology Conference.

Chakrabarti, S. K., and W. A. Tam. 1975. "Interaction of waves with large vertical cylinder." *J. Ship Res.* 19 (1): 23–33.

Chen, L. F., J. Zang, A. J. Hillis, G. C. J. Morgan, and A. R. Plummer. 2014. "Numerical investigation of wave–structure interaction using OpenFOAM." *Ocean Eng.* 88 (Sep): 91–109. https://doi.org/10.1016/j.oceaneng.2014.06.003.

Cong, P., Y. Gou, B. Teng, K. Zhang, and Y. Huang. 2015. "Model experiments on wave elevation around a four-cylinder structure." *Ocean Eng.* 96 (Mar): 40–55. https://doi.org/10.1016/j.oceaneng.2014.11.031.

Contento, G., F. D'Este, M. Sicchiero, R. Codiglia, and M. Calzà. 2005. "Run-up and wave forces on an array of vertical circular cylinders: Experimental study on second-order near trapping." *Int. J. Offshore Polar Eng.* 15 (2): 95–103.

Cozzani, V., M. Campedel, E. Rennia, and E. Krausmann. 2010. "Industrial accidents triggered by flood events: Analysis of past accidents." *J. Hazard. Mater.* 175 (1–3): 501–509. https://doi.org/10.1016/j.jhazmat.2009.10.033.

Eaton, C., and J. Blum. 2017. "*Galena Park gasoline spill dwarfed other Harvey leaks, but stayed out of public eye for days*." *Houston Chronicle*, September 12, 2017.

Ebersole, B. A., T. C. Massey, J. A. Melby, N. C. Nadal-Caraballo, D. L. Hendon, T. W. Richardson, and R. W. Whalin. 2016. *Interim report—Ike Dike concept for reducing hurricane storm surge in the Houston-Galveston region*. Jackson, MS: Jackson State Univ.

Godoy, L. 2007. "Performance of storage tanks in oil facilities damaged by Hurricanes Katrina and Rita." *J. Perform. Constr. Facil.* 21 (6): 441–449. https://doi.org/10.1061/(ASCE)0887-3828(2007)21:6(441).

Hogben, N., and R. G. Standing. 1975. "Experience in computing wave loads on large bodies." In *Proc., 7th Annual Offshore Technology Conf.*, 413–424. Houston: Offshore Technology Conference.

Hope, M. E., et al. 2013. "Hindcast and validation of Hurricane Ike (2008): Waves, forerunner, and storm surge." *J. Geophys. Res. Oceans* 118 (9): 4424–4460. https://doi.org/10.1002/jgrc.20314.

Hu, Z. Z., D. Greaves, and A. Raby. 2016. "Numerical wave tank study of extreme waves and wave-structure interaction using OpenFOAM." *Ocean Eng.* 126 (Nov): 329–342. https://doi.org/10.1016/j.oceaneng.2016.09.017.

Hughes, S. A. 1993. *Physical models and laboratory techniques in coastal engineering*. Singapore: World Scientific.

Ji, X., S. Liu, J. Li, and W. Jia. 2015. "Experimental investigation of the interaction of multidirectional irregular waves with a large cylinder." *Ocean Eng.* 93 (Jan): 64–73. https://doi.org/10.1016/j.oceaneng.2014.10.004.

Johnson, E. R. 1972. *Horizontal forces due to waves acting on large vertical cylinders in deep water*. San Diego: Naval Undersea Center.

Kamath, A., M. A. Chella, H. Bihs, and Ø. A. Arntsen. 2015. "CFD investigations of wave interaction with a pair of large tandem cylinders." *Ocean Eng.* 108 (Nov): 738–748. https://doi.org/10.1016/j.oceaneng.2015.08.049.

Kameshwar, S., and J. E. Padgett. 2018. "Storm surge fragility assessment of aboveground storage tanks." *Struct. Saf.* 70 (Jan): 48–58. https://doi.org/10.1016/j.strusafe.2017.10.002.

Kriebel, D. L. 1987. "A second-order diffraction theory for wave runup and wave forces on a vertical circular cylinder." Ph.D. thesis, Dept. of Coastal and Ocean Engineering, Univ. of Florida.

Kriebel, D. L. 1990. "Nonlinear wave interaction with a vertical circular cylinder. Part I: Diffraction theory." *Ocean Eng.* 17 (4): 345–377. https://doi.org/10.1016/0029-8018(90)90029-6.

Kriebel, D. L. 1992. "Nonlinear wave interaction with a vertical circular cylinder. Part II: Wave run-up." *Ocean Eng.* 19 (1): 75–99. https://doi.org/10.1016/0029-8018(92)90048-9.

Kriebel, D. L. 1998. "Nonlinear wave interaction with a vertical circular cylinder: Wave forces." *Ocean Eng.* 25 (7): 597–605. https://doi.org/10.1016/S0029-8018(97)00029-2.

Laird, A. D. K. 1955. "A model study of wave action on a cylindrical island." *Trans. Am. Geophys. Union* 36 (2): 279–285. https://doi.org/10.1029/TR036i002p00279.

Li, J., Z. Wang, and S. Liu. 2014. "Experimental study of interactions between multi-directional focused wave and vertical circular cylinder. Part II: Wave force." *Coast. Eng.* 83 (Jan): 233–242. https://doi.org/10.1016/j.coastaleng.2013.06.004.

Linton, C. M., and D. V. Evans. 1990. "The interaction of waves with an array of circular cylinders." *J. Fluid Mech.* 215: 549–569. https://doi.org/10.1017/S0022112090002750.

MacCamy, R. C., and R. A. Fuchs. 1954. *Wave forces on piles: A diffraction theory.* Washington, DC: USACE.

McIver, P., and D. V. Evans. 1984. "Approximation of wave forces on cylinder arrays." *Appl. Ocean Res.* 6 (2): 101–107. https://doi.org/10.1016/0141-1187(84)90047-6.

Mogridge, G. R., and W. W. Jamieson. 1976. *Wave loads on large circular cylinders: A design method*. Ottawa: National Research Council of Canada.

Morison, J. R., J. W. Johnson, and S. A. Schaaf. 1950. "The force exerted by surface waves on piles." *J. Pet. Technol.* 189 (5): 149–154. https://doi.org/10.2118/950149-G.

Nagai, S. 1973. "Wave forces on structures." In Vol. 9 of *Advances in hydroscience*, 253–324. New York: Academic Press.

Neelamani, S., V. Sondar, and C. P. Vendhan. 1989. "Dynamic pressure distribution on a cylinder due to wave diffraction." *Ocean Eng.* 16 (4): 343–353. https://doi.org/10.1016/0029-8018(89)90012-7.

Niedzwecki, J. M., and A. S. Duggal. 1992. "Wave runup and forces on cylinders in regular and random waves." *J. Waterw. Port Coastal Ocean Eng.* 118 (6): 615–634. https://doi.org/10.1061/(ASCE)0733-950X(1992)118:6(615).

Ohl, C. O. G., P. H. Taylor, R. E. Taylor, and A. G. L. Borthwick. 2001b. "Water wave diffraction by a cylinder array. Part 2: Irregular waves." *J. Fluid Mech.* 442: 33–66. https://doi.org/10.1017/S0022112001004943.

Ohl, C. O. G., R. E. Taylor, P. H. Taylor, and A. G. L. Borthwick. 2001a. "Water wave diffraction by a cylinder array. Part 1: Regular waves." *J. Fluid Mech.* 442: 1–32. https://doi.org/10.1017/S0022112001004931.

Rahman, M., and H. S. Heaps. 1983. "Wave forces on offshore structures: Nonlinear wave diffraction by large cylinders." *J. Phys. Oceanogr.* 13 (12): 2225–2235. https://doi.org/10.1175/1520-0485(1983)013<2225:WFOOSN>2.0.CO;2.

Rathje, E., et al. 2017. "DesignSafe: A new cyberinfrastructure for natural hazards engineering." *Nat. Hazard. Rev.* 18 (3): 06017001. https://doi.org/10.1061/(ASCE)NH.1527-6996.0000246.

USACE. 2008. *Coastal engineering manual—Part II*. Washington, DC: USACE.

Wang, C. Z., and G. X. Wu. 2010. "Interactions between fully nonlinear water waves and cylinder arrays in a wave tank." *Ocean Eng.* 37 (4): 400–417. https://doi.org/10.1016/j.oceaneng.2009.12.006.